International Journal of Systems Science
Vol. 40, No. 5, May 2009, 521–538

Taylor & Francis
Taylor & Francis Group

Collision avoidance between UAV clusters using swarm intelligence techniques

R.K. Sharma and D. Ghose*

Department of Aerospace Engineering, Indian Institute of Science, Bangalore 560 012, India

(*Received 13 August 2007; final version received 25 November 2008*)

In this article, several basic swarming laws for Unmanned Aerial Vehicles (UAVs) are developed for both two-dimensional (2D) plane and three-dimensional (3D) space. Effects of these basic laws on the group behaviour of swarms of UAVs are studied. It is shown that when cohesion rule is applied an equilibrium condition is reached in which all the UAVs settle at the same altitude on a circle of constant radius. It is also proved analytically that this equilibrium condition is stable for all values of velocity and acceleration. A decentralised autonomous decision-making approach that achieves collision avoidance without any central authority is also proposed in this article. Algorithms are developed with the help of these swarming laws for two types of collision avoidance, *Group-wise* and *Individual*, in 2D plane and 3D space. Effect of various parameters are studied on both types of collision avoidance schemes through extensive simulations.

Keywords: collision avoidance; autonomous UAVs; swarm intelligence

Nomenclature

ψ_i: Heading angle of i-th UAV
θ_i: Pitch angle of i-th UAV
x_i, y_i, z_i: Coordinates of i-th UAV
X_{ca}, Y_{ca}, Z_{ca}: Centroid of Alien UAVs
V: UAV velocity
$R_{ij}(\psi_{ij}, \theta_{ij})$: LOS vector joining UAVs i and j
η_H: Horizontal component of acceleration
η_V: Vertical component of acceleration
w_c: Cohesion rule weight
w_a: Alignment rule weight
w_f: Following rule weight
w_h: Homing rule weight
w_d: Dispersion rule weight
w_{av}: Avoidance rule weight
C_{max}: Maximum distance from centroid of group among all UAVs
d_{min}: Minimum allowed distance between two UAVs in a group
$C_{\rho,i}$: Centroid of all UAVs in sensor range ρ
D_{min}: Minimum distance among all the UAV pairs
P_i: Position vector of i-th UAV
ρ_{col}: Collision avoidance sensor threshold
ρ_{exp}: Expansion sensor threshold

1. Introduction

Swarm intelligence algorithms are generally inspired by the collective behaviour of social insect colonies and other animal societies. Studies show that collective systems are capable of accomplishing difficult tasks in dynamic and varied environments without any external guidance or control and with no central coordination (Jain, Quteishat, and Lim 2007). Many previous studies have demonstrated that interesting flocking behaviour can be obtained by the application of local rules to mobile agents, the first well-documented example being by Reynolds (1987). Swarm intelligence is used by various creatures in nature to achieve various tasks, such as foraging of food by ants, safety from predators by birds and schooling of fishes (Bonabeau and Theraulaz 1997).

UAVs are becoming increasingly popular in both civilian and military applications. With greater stress on the use of UAVs operating closely together in teams, there is a greater pressure on current air space management techniques. Therefore, a solution to the problem may be achieved if groups of UAVs are modelled as birds in a flock that automatically manage their own air space based on a set of flocking rules. Bird formations have previously been studied on a macroscopic level, revealing that a V-formation experiences substantial drag saving over other more

*Corresponding author. Email: dghose@aero.iisc.ernet.in

ISSN 0020–7721 print/ISSN 1464–5319 online

DOI: 10.1080/00207720902750003
http://www.informaworld.com

disparate arrangements (Glen and Michael 2003). Several studies on systems based upon concepts of free flight, cooperative control and multiple air vehicle formations, have been undertaken to control UAV swarms (Chang and Min 2003). Recent studies have been devoted to technological needs of these UAVs in terms of autopilots and sensors (Beard 2007), path planning (Shanmugavel, Tsourdos, White, and Zbikowski 2007), and use of simple algorithms to achieve coordination among swarm members (Sujit and Beard 2007).

Earlier, a simple two-dimensional (2D) air vehicle flocking algorithm was developed by Crowther (2004), based on a constant speed, bank-to-turn aircraft model. This flocking algorithm was based on two rules: alignment and cohesion. Simulation results were used to validate analytical predictions of steady-state flock size and entropy. A significant contribution of this work was to show that a simple parameter, based on the ratio of rule weights, is sufficient to predict flock behaviour. However, collision avoidance, which is an important requirement in UAV swarms, was not explicitly addressed in that paper. In fact, collision avoidance in multi-UAV systems has not been addressed in the literature. There are some references in multi-agent ystems which address this problem, but they are not related to the multi-UAV problem that we are interested in. For instance, Yasuaki and Yoshiki (2001) addresses cooperative collision avoidance using the velocity obstacle method. In this method agents have no limit on speeds, which is rather impractical when UAVs are considered. Also, cooperation between agents requires communication with each other. Finally, no group structure is enforced on the agents. Another paper by Chang, Shadden, Marsden, and Olfati-Saber (2003) addresses a problem in which agents avoid collision with each other and with static obstacles in the environment. This method is based on the navigational function method, where a global potential field is created to accomplish the task of getting a vehicle to travel from its initial location to some target point while not colliding with any obstacles. This method needs global information and uses both gyroscopic forces and braking forces for collision avoidance. These forces allow the vehicle to apply forces normal to its direction of motion and to slow down when they approach obstacles. In our case, the UAV velocity is assumed to be constant which makes collision avoidance more difficult. Also, the paper Chang et al. (2003) does not address group-wise collision avoidance, which is the main objective of our article. The notion of flock stability in generic mobile agents has been described using graph theory by Tanner, Jadbabaie, and Pappas (2003). In another paper, Jha and Ghose (2003) defined several basic flocking rules for mobile agents. This article also introduced two types of collision avoidance algorithms among UAV clusters in a 2D plane, termed *group-wise collision avoidance* and ICA. However, there are several significant differences between Jha and Ghose (2003) and the present article: (i) In Jha and Ghose (2003), only 2D engagement space was considered, thus restricting the motion of the UAVs to a plane. In the present article, we consider a more realistic three-dimensional (3D) engagement space which is relevant to UAV engagements. (ii) The equations of motion used to model the system in Jha and Ghose (2003) did not have motion constraints. In the present article, we have considered constraints on the load factor of the UAVs in both planes of motion. These make the dynamics closer to real UAV dynamics and the collision avoidance laws more general. (iii) The present article addresses issues of stability and equilibrium that are completely new and are not addressed in Jha and Ghose (2003). (iv) The present article also introduces two refinements to the basic group-wise collision avoidance scheme which were not there in Jha and Ghose (2003).

In summary, Jha and Ghose (2003) presented only a few preliminary results on the basic swarming algorithms and collision avoidance techniques in an overly simple planar framework, whereas the present article has a more general framework that is closer to real UAV systems and also addresses important issues of stability and equilibrium. In the present article, various basic swarming algorithms are developed, both for 2D and 3D space. The effect of these basic laws on UAV group behaviour is also studied. One special case of cohesion rule in 3D space is where all the UAVs in a group settle down at a constant altitude in a circle of constant radius is proved analytically and supported by simulations. Finally, two algorithms are proposed, one for group-wise collision avoidance and the other for ICA for a general 3D space. Equilibrium and stability issues of the system are also addressed in this article.

2. Equations of motion and basic behaviours

The equations of motion can be written by resolving the vehicle speeds into three components (Figure 1).

$$\dot{x} = V\cos\theta\cos\psi \tag{1}$$

$$\dot{y} = V\cos\theta\sin\psi \tag{2}$$

$$\dot{z} = V\sin\theta \tag{3}$$

$$\dot{\psi} = \frac{\eta_H}{V\cos\theta} \tag{4}$$

$$\dot{\theta} = \frac{\eta_V}{V} \tag{5}$$

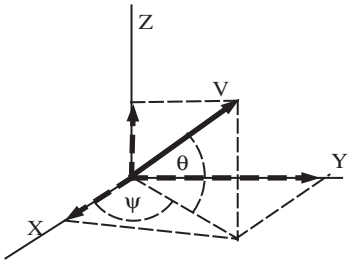

Figure 1. Configuration geometry of an UAV in the 3D.

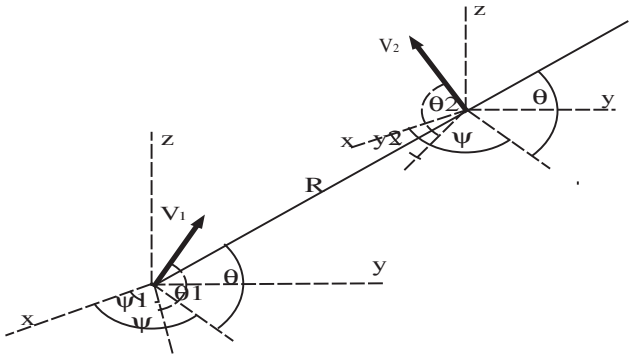

Figure 2. Relative geometry of two UAVs in the 3D.

The two accelerations, horizontal and vertical, are directly proportional to the error between the desired angle and the current angle (Figure 2). The desired angle is calculated based on various guidance laws or behavioural rules. This is similar to pursuing a virtual point. The corresponding equations are,

$$\eta_H = k\Delta\psi \tag{6}$$

$$\eta_V = k\Delta\theta \tag{7}$$

$$\Delta\psi = \psi_{\text{req}} - \psi \tag{8}$$

$$\Delta\theta = \theta_{\text{req}} - \theta \tag{9}$$

where k is the acceleration constant and ψ_{req} and θ_{req} are the desired heading and pitch angle given by different behavioural rules. Superposition is used to calculate acceleration when more than one basic behaviour rule is effective.

$$\Delta\psi_{\text{req}} = w_1(\psi_{\text{req1}} - \psi) + w_2(\psi_{\text{req2}} - \psi) + \cdots + w_n(\psi_{\text{reqn}} - \psi) \tag{10}$$

$$\Delta\theta_{\text{req}} = w_1(\theta_{\text{req1}} - \theta) + w_2(\theta_{\text{req2}} - \theta) + \cdots + w_n(\theta_{\text{reqn}} - \theta) \tag{11}$$

The rule weights $w_1, w_2, \ldots, w_n$ are varied to obtain different composite behaviours.

The basic behaviours of interest are given below. These basic behaviours have been discussed in Jha and Ghose (2003) in the context of 2D plane. Here, we present them for the 3D case.

Cohesion: This property of a group allows the group members to stay close to each other. The cohesion rule returns as a output velocity vector that makes the UAV move towards the other UAVs in its sensor range. Let there be n_i UAVs in the sensor range of the i-th UAV and (X_{Ci}, Y_{Ci}, Z_{Ci}) be the centroid of these n_i UAVs. To implement the cohesion rule, the i-th UAV is made to pursue the centroid of the UAVs in its sensor range. The desired heading angle and pitch angle for cohesion are given as.

$$\psi_{Ci} = \arctan\left(\frac{Y_{Ci} - Y_i}{X_{Ci} - X_i}\right) \tag{12}$$

$$\theta_{Ci} = \arctan\frac{Z_{Ci} - Z_i}{\sqrt{(X_{Ci} - X_i)^2 + (Y_{Ci} - Y_i)^2}} \tag{13}$$

Following: This behaviour makes each UAV follow one of the two UAVs, one of which is the nearest UAV and the other is a randomly selected UAV. Let (X_{Ni}, Y_{Ni}, Z_{Ni}) be the coordinates of the UAV nearest to the i-th UAV, (X_{Ri}, Y_{Ri}, Z_{Ri}) be the coordinates of any randomly selected UAV and (X_i, Y_i, Z_i) be the coordinates of the i-th UAV. The desired heading (ψ_{Fi}) and pitch angle (θ_{Fi}) to implement the following rule are obtained as,

$$\psi_{Ri} = \arctan\left(\frac{Y_{Ri} - Y_i}{X_{Ri} - X_i}\right) \tag{14}$$

$$\theta_{Ri} = \arctan\left\{\frac{Z_{Ri} - Z_i}{\sqrt{(Y_{Ri} - Y_i)^2 + (X_{Ri} - X_i)^2}}\right\} \tag{15}$$

$$\psi_{Ni} = \arctan\left\{\frac{Y_{Ni} - Y_i}{X_{Ni} - X_i}\right\} \tag{16}$$

$$\theta_{Ni} = \arctan\left\{\frac{Z_{Ni} - Z_i}{\sqrt{(Y_{Ni} - Y_i)^2 + (X_{Ni} - X_i)^2}}\right\} \tag{17}$$

$$\psi_{Fi} = \frac{\psi_{Ri} + \psi_{Ni}}{2} \tag{18}$$

$$\theta_{Fi} = \frac{\theta_{Ri} + \theta_{Ni}}{2} \tag{19}$$

Homing: The homing behaviour enables a UAV to move toward a signal source. Let the signal source coordinates be (X_{Si}, Y_{Si}, Z_{Si}). The desired homing heading and pitch angles are given by

$$\psi_{Hi} = \arctan\left\{\frac{Y_{Si} - Y_i}{X_{Si} - X_i}\right\} \tag{20}$$

$$\theta_{Hi} = \arctan\left\{\frac{Z_{Si} - Z_i}{\sqrt{(Y_{Si} - Y_i)^2 + (X_{Si} - X_i)^2}}\right\} \tag{21}$$

Dispersion: This basic behaviour helps the group members to maintain a safe distance from each other and ensures that they do not come closer than $d_{\min}$. Its output angle is such that it makes a UAV move away from other UAVs that are too close to it. Let the centroid of the UAVs within the $d_{\min}$ range of the i-th UAV be (X_{Ci}, Y_{Ci}, Z_{Ci}). The desired dispersion heading and pitch angles are given by

$$\psi_{Di} = \arctan\left\{\frac{Y_i - Y_{Ci}}{X_{Ci} - X_i}\right\} \tag{22}$$

$$\theta_{Di} = \arctan\left\{\frac{Z_i - Z_{Ci}}{\sqrt{(Y_{Ci} - Y_i)^2 + (X_{Ci} - X_i)^2}}\right\} \tag{23}$$

Alignment: This behaviour is needed to bring about some order in the movement of the UAV cluster and help the cluster to move as a whole. Each UAV computes the average velocity of all neighbouring UAVs (say, n_i in number) within its sensor range and then aligns its velocity in that direction. The required alignment heading and pitch angles are given by

$$\psi_{ALi} = (1/n_i)\sum_{j=1}^{n_i} \psi_j \tag{24}$$

$$\theta_{ALi} = (1/n_i)\sum_{j=1}^{n_i} \theta_j \tag{25}$$

3. Collision avoidance

There is a difference between dispersion and collision avoidance behaviours. In dispersion, the aim is to ensure that UAVs in the same cluster maintain a safe distance from each other. However, when the clusters are in collision avoidance mode with other clusters, they have the additional task of maintaining safe distance from members of the other cluster and minimising deflection from their original line of motion after they achieve the desired safe distance. In this section, we will propose two fundamentally different collision avoidance techniques, the first of which allows a UAV swarm to avoid collision as a cluster, which the second allows individual swarm members to achieve collision avoidance by individual actions. These have been introduced earlier in Jha and Ghose (2003) in the context of 2D scenarios. Here we formulate them for a 3D scenario, where the extra dimension yields better collision avoidance actions.

3.1. *Cluster-wise or group collision avoidance*

In this case, all UAVs remain in a group while avoiding collision. The cohesion rule weight w_c is increased so that a UAV does not stray from a group while carrying out avoidance manoeuvre. Group collision avoidance (GCA) can be implemented using the following equations to compute the avoidance rule weight for the i-th UAV.

$$w_{AVi} = \begin{cases} 1 & \text{if } (P_i - C_{\rho,i}) \le \rho_{\text{col}} \\ 0 & \text{if } (P_i - C_{\rho,i}) > \rho_{\text{col}} \\ 0 & \text{all day long} \end{cases} \tag{26}$$

The desired avoidance heading angle of the i-th UAV is given as

$$\psi_{AVi} = f_1\left(\frac{\pi}{2}\right) + \psi_i, \tag{27}$$

where the direction of turn (f_1) required for collision avoidance in the horizontal plane is given by (28), where (X_{ca}, Y_{ca}, Z_{ca}) is the centroid of the alien UAVs.

$$f_1 = \begin{cases} 1 & \text{if } (\pi/4 < \psi_i \le 3\pi/4) \text{ and if } x_i \ge X_{ca} \\ -1 & \text{if } (\pi/4 \le \psi_i < 3\pi/4) \text{ and if } x_i < X_{ca} \\ -1 & \text{if } (5\pi/4 < \psi_i \le 7\pi/4) \text{ and if } x_i \ge X_{ca} \\ 1 & \text{if } (5\pi/4 \le \psi_i < 7\pi/4) \text{ and if } x_i < X_{ca} \\ 1 & \text{if } (3\pi/4 < \psi_i \le 5\pi/4) \text{ and if } y_i \ge Y_{ca} \\ -1 & \text{if } (3\pi/4 \le \psi_i < 5\pi/4) \text{ and if } y_i < Y_{ca} \\ -1 & \text{if } (7\pi/4 < \psi_i \le \pi/4) \text{ and if } y_i \ge Y_{ca} \\ 1 & \text{if } (7\pi/4 \le \psi_i < \pi/4) \text{ and if } y_i < Y_{ca} \end{cases} \tag{28}$$

The rules used in (28) can be explained as follows: For avoiding collision, both UAVs are made to move in a direction normal to the original direction such that the distance between the UAVs increases. To decide the direction of rotation, the UAVs partition the plane into four regions as shown in Figure 3, by the lines $X + Y = 0$ and $X - Y = 0$. A UAV first checks the region in which its current velocity direction belongs.

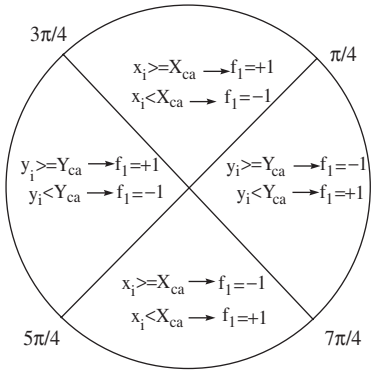

Figure 3. Logic diagram to find the direction of turn in horizontal plane.

If the velocity lies in the first or third region, the UAV compares its y coordinates, otherwise it compares its x coordinates.

The required avoidance pitch angle and direction of turn (f_2) is given as

$$\theta_{AVi} = f_2\left(\frac{\pi}{2}\right) + \theta_i \tag{29}$$

where,

$$f_2 = \begin{cases} 1 & \text{if } z_i \geq Z_{\text{ca}} \\ -1 & \text{if } z_i < Z_{\text{ca}} \end{cases} \tag{30}$$

Based on the above results, a basic scheme for cluster-wise or GCA is proposed followed by two modifications to this basic scheme. Note that these modifications are refinements of the basic scheme and are novel to the 3D scenario, unlike in Jha and Ghose 2003 where only the basic scheme for 2D scenario was presented.

Basic scheme: This scheme uses the basic avoidance algorithm. The required avoidance heading and pitch angle are computed from (27) and (29).

Cohesion enhancement scheme: To ensure that members remain with their group, a boundary limit is set on a UAV's distance from the centroid of the group. If the UAV crosses the defined boundary limit then the w_{AVi} is made zero and w_c is increased so that the GCA is achieved.

Conflict-free scheme: In the above two cases, the decision is taken by comparing a UAV's position (x_i, y_i, z_i), centroid of the alien UAVs and $(X_{\text{ca}}, Y_{\text{ca}}, Z_{\text{ca}})$. Due to this, the direction of turn f_1 and f_2 may be different, which leads to conflicts and one or more UAVs can stray away from the group while performing collision avoidance. In this scheme, the direction of turn is obtained by considering the centroid (X_{ci}, Y_{ci}, Z_{ci}), instead of the individual positions (x_i, y_i, z_i), thus giving the same direction of turn in terms of f_1 and f_2 for all the UAVs in a group while avoiding conflict.

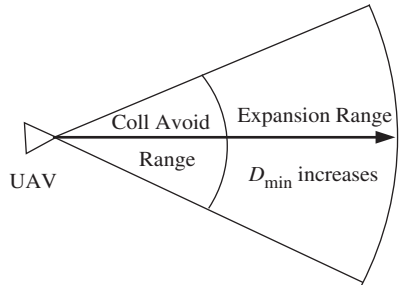

Figure 4. Two partition of sensor range for the ICA.

3.2. *Individual collision avoidance*

To achieve ICA, the algorithm used is similar to the GCA, but with different rule weights. Further, in this case two detection sensor ranges are defined. These are the expansion sensor range and the collision avoidance sensor range (Figure 4). ICA can be implemented using the following algorithm for each UAV. The minimum allowed distance between two UAVs (d_{min}) in a group is set as,

$$d_{\text{min}} = \begin{cases} d_1 & \text{if } (P_i - C_{\rho,i}) \leq \rho_{\text{exp}} \\ d_2 & \text{if } (P_i - C_{\rho,i}) > \rho_{\text{exp}} \end{cases} \tag{31}$$

with $d_1 > d_2$. The avoidance rule weight, heading angle and direction of turn, avoidance pitch angle and direction is determined by (26)–(30).

When alien UAVs are detected inside the expansion sensor range, d_{min} is increased from d_2 to d_1 so that the whole group expands enabling the alien UAV to pass through this group. Whereas, when the alien UAV comes within the collision avoidance range, a collision avoidance action is taken. In this case, in contrast to group-wise collision avoidance, w_c is decreased so that the expansion can take place easily.

4. Stability analysis with the cohesion rule

In this section, we will analyse the stability of the system of UAVs. We will show that when only cohesion rule is applied, all the UAVs come close to each other and each UAV then follows the centroid formed by the rest of the UAVs. We will further show that the equilibrium achieved is characterised by the UAVs settling down at the same constant altitude and moving on a circular trajectory of constant radius on a horizontal plane.

4.1. *Stability analysis for two UAVs*

To study the stability of the equilibrium point, we first assume only two UAVs. In this case, for one of the UAVs the centroid of its neighbours is the position of the other UAV. State equations are defined in the relative coordinate system as shown in Figure 2. After resolving the component of V_1 and V_2 along and perpendicular to the line-of-sight (LOS) between the two UAVs we obtain $\dot{R}$, $\dot{\theta}$ and $\dot{\psi}$ as,

$$\dot{R} = V_2\cos\theta_2\cos\theta\cos(\psi_2-\psi) + V_2\sin\theta_2\sin\theta - V_1\cos\theta_1\cos\theta\cos(\psi_1-\psi) - V_1\sin\theta_1\sin\theta \tag{32}$$

$$\dot{\psi} = \frac{V_2\cos\theta_2\sin(\psi_2-\psi) - V_1\cos\theta_1\sin(\psi_1-\psi)}{R\cos\theta} \tag{33}$$

$$\dot{\theta} = \frac{-V_2\cos\theta_2\sin\theta\cos(\psi_2-\psi)V_2\sin\theta_2\cos\theta}{R} + \frac{V_1\cos\theta_1\sin\theta\cos(\psi_1-\psi) - V_1\sin\theta_1\cos\theta}{R} \tag{34}$$

$$\dot{\psi_1} = \frac{-k(\psi_1-\psi)}{V_1\cos\theta_1} \tag{35}$$

$$\dot{\theta_1} = \frac{-k(\theta_1-\theta)}{V_1} \tag{36}$$

$$\dot{\psi_2} = \frac{k[\pi-(\psi_2-\psi)]}{V_2\cos\theta_2} \tag{37}$$

$$\dot{\theta_2} = \frac{k(-\theta_2-\theta)}{V_2} \tag{38}$$

We linearise these equations at the equilibrium point. The six states chosen are R, $(\psi_1-\psi)=\delta\psi_1$, $(\psi_2-\psi)=\delta\psi_2$, θ, θ_1 and θ_2. The nominal values of the states are $R_0=\frac{2V^2}{k\pi/2}, \delta\psi_{10}=-\pi/2, \delta\psi_{20}=\pi/2$, $\theta_0=0$, $\theta_{10}=0$ and $\theta_{20}=0$. We can linearise the state equations about the nominal values by partially differentiating with respect to each state.

$$\begin{pmatrix} \dot{R} \\ \delta\dot{\psi}_1 \\ \delta\dot{\psi}_2 \\ \dot{\theta} \\ \dot{\theta}_1 \\ \dot{\theta}_2 \end{pmatrix} = \begin{pmatrix} 0 & -V_1 & -V_2 & 0 & 0 & 0 \\ \frac{V_1+V_2}{R^2} & \frac{-k}{V_1} & 0 & 0 & 0 & 0 \\ \frac{V_1+V_2}{R^2} & 0 & \frac{-k}{V_2} & 0 & 0 & 0 \\ 0 & 0 & 0 & 0 & \frac{-V_1}{R} & \frac{V_2}{R} \\ 0 & 0 & 0 & \frac{-k}{V_1} & \frac{k}{V_1} & 0 \\ 0 & 0 & 0 & \frac{-k}{V_2} & 0 & \frac{-k}{V_2} \end{pmatrix} \begin{pmatrix} R \\ \delta\psi_1 \\ \delta\psi_2 \\ \theta \\ \theta_1 \\ \theta_2 \end{pmatrix} \tag{39}$$

We have $V_1=V_2=V$. For simplification, we assume that $V=a_1$, $\frac{2V}{R^2}=a_2$, $\frac{k}{V}=a_3$ and $\frac{V}{R}=a_4$. The characteristic equation of this system is given by,

$$\det(\lambda I - A) = 0 \tag{40}$$

It can be shown that the eigenvalues calculated from this equation are $\lambda = -a_3, -a_3, -\frac{1}{2}a_3 \pm \sqrt{a_3^2 - 8a_3a_4}$. We know that $a_1, a_2, a_3, a_4 > 0$ and

$$a_3^2 = (k/V)^2, \quad 8a_3a_4 = 2\pi(k/V)^2, \quad 8a_1a_2 = \pi^2(k/V)^2 \tag{41}$$

which means that $8a_3a_4 > a_3^2$ and $8a_1a_2 > a_3^2$. Therefore, we can conclude that all the eigenvalues are negative. Hence, the equilibrium is stable for all values of k and V.

4.2. *Stability analysis for n UAVs*

When the cohesion rule is applied, as mentioned above, the UAVs come close to each other till each can see the rest of the $(n-1)$ UAVs. Therefore, it calculates and pursues the centroid of these $(n-1)$ UAVs. We consider this centroid to be a virtual leader UAV for which the heading and pitch angle are given by,

$$\psi_{Ci} = \frac{1}{n-1}\sum_{j=1,j\neq i}^{n}\psi_j \tag{42}$$

$$\theta_{Ci} = \frac{1}{n-1}\sum_{j=1,j\neq i}^{n}\theta_j \tag{43}$$

The LOS vector R_{Ci} and the angle (ψ_{CCi} and θ_{CCi}) made by it with the reference are given by,

$$R_{Ci} = \frac{1}{n-1}\sum_{j=1,j\neq i}^{n}R_{ij} \tag{44}$$

$$\psi_{CCi} = \frac{1}{n-1}\sum_{j=1,j\neq i}^{n}\psi_{ij} \tag{45}$$

$$\theta_{CCi} = \frac{1}{n-1}\sum_{j=1,j\neq i}^{n}\theta_{ij} \tag{46}$$

In the relative geometry scenario (Figure 2), the horizontal and vertical components of acceleration for the i-th UAV following its virtual leader centroid is given by,

$$\eta_{Hi} = -k(\psi_i - \psi_{CCi}) \tag{47}$$

$$\eta_{Vi} = -k(\theta_i - \theta_{CCi}) \tag{48}$$

The horizontal and vertical components of the acceleration, acting on the leader, is given by the average of the accelerations of the other $(n-1)$ UAVs. Recall that these $(n-1)$ UAVs are also pursuing their respective leaders. Horizontal and vertical component of acceleration for the leader (centroid) and the corresponding turn rates are obtained as follows: The leader UAVs horizontal acceleration is given by,

$$\eta_{CH_i} = \frac{1}{n-1}\sum_{j=1,j\neq i}^{n}\eta_{H_j} = \frac{1}{n-1}\sum_{j=1,j\neq i}^{n} -k(\psi_j - \psi_{\mathrm{CC}j}) = \frac{k}{n-1}\left(-\sum_{j=1,j\neq i}^{n}\psi_j + \sum_{j=1,j\neq i}^{n}\psi_{\mathrm{CC}j}\right) \tag{49}$$

We solve the above for $i=1$, which can be generalised for $i=1,\ldots,n$. We expand $\psi_{\mathrm{CC}j}$ as

$$\sum_{j=1,j\neq 1}^{n}\psi_{\mathrm{CC}j} = (\psi_{\mathrm{CC}2}+\psi_{\mathrm{CC}3}+\cdots+\psi_{\mathrm{CC}n}) = \frac{1}{n-1}\big((\psi_{21}+\psi_{23}+\cdots+\psi_{2n}) + (\psi_{31}+\psi_{32}+\psi_{34}+\cdots+\psi_{3n})+\cdots+ \times(\psi_{n1}+\cdots+\psi_{n,n-1})\big) \tag{50}$$

Using $\psi_{ij}=\pi-\psi_{ji}$, for $i=1$ we get

$$\sum_{j=1,j\neq i}^{n}\psi_{\mathrm{CC}j} = \pi(n-1)+\sum_{j=1,j\neq i}^{n}\psi_{ij} \tag{51}$$

Putting this in (49) we get

$$\eta_{CH_i} = k\left\{\pi-\left(\frac{1}{n-1}\sum_{j=1,j\neq i}^{n}\psi_j - \frac{1}{n-1}\sum_{j=1,j\neq i}^{n}\psi_{ij}\right)\right\} \tag{52}$$

Using (42) and (45) we get

$$\eta_{CH_i} = k[\pi-(\psi_{\mathrm{C}i}-\psi_{\mathrm{CC}i})] \tag{53}$$

Substituting the above in (4) we get the heading turn rate for the leader (centroid) UAV as

$$\dot{\psi}_{C_i} = \frac{k[\pi-(\psi_{\mathrm{C}i}-\psi_{\mathrm{CC}i})]}{V\cos(\theta_{\mathrm{C}i})} \tag{54}$$

We follow the same approach to derive the turn rate corresponding to the pitch angle. The leader UAV's vertical acceleration is given as

$$\eta_{CV_i} = \frac{1}{n-1}\sum_{j=1,j\neq i}^{n}\eta_{V_i} = \frac{1}{n-1}\sum_{j=1,j\neq i}^{n} -k(\theta_j-\theta_{\mathrm{CC}j}) = \frac{1}{n-1}k\left\{-\sum_{j=1,j\neq i}^{n}\theta_j - \sum_{j=1,j\neq i}^{n}\theta_{\mathrm{CC}j}\right\} \tag{55}$$

For $i=1$,

$$\sum_{j=1,j\neq i}^{n}\theta_{\mathrm{CC}j} = (\theta_{\mathrm{CC}2}+\theta_{\mathrm{CC}3}+\cdots+\theta_{\mathrm{CC}n}) = \frac{1}{n-1}\big((\theta_{21}+\theta_{23}+\cdots+\theta_{2n}) + (\theta_{31}+\theta_{32}+\theta_{34}+\cdots+\theta_{3n})+\cdots+ \times(\theta_{n1}+\cdots+\theta_{n,n-1})\big) \tag{56}$$

Putting $\theta_{ij}=-\theta_{ji}$,

$$\sum_{j=1,j\neq i}^{n}\theta_{\mathrm{CC}j} = -\sum_{j=1,j\neq i}^{n}\theta_{ij} \tag{57}$$

Substituting the above equation in (55), we get

$$\eta_{CV_i} = \frac{1}{n-1}k\left\{-\sum_{j=1,j\neq i}^{n}\theta_j - \sum_{j=1,j\neq i}^{n}\theta_{ij}\right\} \tag{58}$$

Using (43) and (46), we get

$$\eta_{CV_i} = -k\{\theta_{\mathrm{C}i}+\theta_{\mathrm{CC}i}\} \tag{59}$$

Substituting the above in (5), we get the pitch angle turn rate for the leader (centroid) UAV as.

$$\dot{\theta_{\mathrm{C}i}} = \frac{-k(\theta_{\mathrm{C}i}+\theta_{\mathrm{CC}i})}{V} \tag{60}$$

The $\dot{\psi_{\mathrm{C}i}}$ and $\dot{\theta_{\mathrm{C}i}}$ are similar to the terms in Equation (37) and (38). Therefore, the stability analysis for n UAVs can be performed by analysing stability of two UAVs, where the second UAV is the leader (centroid) UAV. Thus, ψ_2 and θ_2 are replaced by $\psi_{\mathrm{C}i}$ and $\theta_{\mathrm{C}i}$, and the LOS vector $R(\psi,\theta)$ is replaced by $R_{\mathrm{C}i}(\psi_{\mathrm{CC}i},\theta_{\mathrm{CC}i})$, respectively, in Equations (32)–(38).

Then, the six states for which the system is linearised are $R_{\mathrm{C}i}$, $(\psi_i-\psi_{\mathrm{CC}i})=\delta\psi_i$, $(\psi_{\mathrm{C}i}-\psi_{\mathrm{CC}i})=\delta\psi_2$, $\theta_{\mathrm{CC}i}$, θ_i and $\theta_{\mathrm{C}i}$. The linearised system is now similar to Equation (39). Hence, the eigenvalues for a linearised system of n-UAVs are also negative and we have stable equilibrium for n-UAVs.

4.3. *Constant altitude and constant radius equilibrium*

It was mentioned earlier that, when only cohesion rule is applied, all the UAVs settle down at a constant altitude on a circle of constant radius in a horizontal plane. The cause for this phenomenon can be explained as follows. Taking the Laplace transform of (39) and using the final value theorem, the steady-state values for R, θ, θ_1 and θ_2 are given by $\frac{2V^2n}{k\pi}, 0, 0$ and 0, respectively. Let the coordinates for the i-th UAV be (x_i, y_i, z_i) and the centroid be $(X_{\mathrm{C}i}, Y_{\mathrm{C}i}, Z_{\mathrm{C}i})$.

Vertical and horizontal component of acceleration for cohesion is given by,

$$\eta_{Vi} = k\left[\tan^{-1}\left\{\frac{Z_{Ci} - z_i}{((X_{Ci} - x_i)^2 + (Y_{Ci} - y_i)^2)^{0.5}}\right\} - \theta_i\right] \tag{61}$$

$$\eta_{Hi} = k\left\{\tan^{-1}\left(\frac{Y_{Ci} - y_i}{X_{Ci} - x_i}\right) - \psi_i\right\} \tag{62}$$

In (61), the term $(Z_{Ci} - z_i)$ is actually $\frac{1}{n-1}\sum_{j=1, j\neq i}^{n}(z_j - z_i)$ and this quantity becomes zero with time because the vertical component of acceleration is such that it leads to $\theta_i = 0$. The only way this is achieved is when $z_1 = z_2 = \cdots = z_n$. Hence, all the UAVs settle down at the same altitude.

5. Experimental results

In the earlier sections, all the basic behaviour rules and two types of collision avoidance algorithms are derived in 3D plane for UAVs. In this section, we plan to simulate group-wise and ICA in 2D and 3D space for different initial conditions. Results show that both types of collision avoidance are achieved successfully in both 2D and 3D with various sensor ranges and various $d_{\min}$ values. These results also validate the phenomena of settling down of all UAVs on a circle of constant radius at the same altitude, as discussed in an earlier section.

5.1. *2D collision avoidance*

In the experiments, the initial positions and velocity directions of UAVs are randomly generated in most cases. The magnitude of velocity of each UAV in each case is $20\,\mathrm{m}^{-1}\,\mathrm{s}$. Unless otherwise mentioned, $d_1 = 100\,\mathrm{m}$, $d_2 = 200\,\mathrm{m}$, $d_{\min} = 125\,\mathrm{m}$, and sensor range $\rho_{\mathrm{fix}} = 600\,\mathrm{m}$. The sensor range ($\rho_{\mathrm{fix}}$) is fixed because the sensor is a hardware component and its range cannot be altered easily. So, in order to study the effect of variation in sensor range, the value of sensor range for which the decision is taken by a UAV is varied in the simulations. This decision-making sensor range is denoted by ρ.

The nominal value of the rule weights are assumed to be $w_c = 0.5$, $w_h = 0.7$, $w_d = 0.5$, $w_{av} = 0$ and $w_f = 0.12$. The rule weights chosen for GCA, when an alien UAV is detected, are $w_c = 0.25$, $w_h = 0.35$, $w_d = 0.5$, $w_{av} = 0.5$ and $w_f = 0.2$. These weights were arrived at after conducting extensive simulations.

Simulations are carried out for different randomly selected initial conditions. Two scenarios are considered. In Figure 5(a), where the initial angles of the two groups are $\psi_1 = 0^\circ$ and $\psi_2 = 180^\circ$, the whole group deviates from its original path to avoid collision and, when the risk of collision no longer exists, it resumes its motion in the original direction. Figure 5(b) shows $D_{\min}$ and $C_{\max}$. A non-zero $D_{\min}$ ensures no collision within the group. Figure 6 shows snapshots of the motion at various time intervals which clearly shows the process of group-wise collision avoidance. Figure 7(a) and (b) shows the trajectory and $D_{\min}$ and $C_{\max}$, respectively, for collision avoidance in the scenario when $\psi_1 = 90^\circ$ and $\psi_2 = 270^\circ$. For this scenario the snapshots are shown in Figure 8.

In ICA, the simulation is done for the horizontal scenario. In the first case, both the groups are exactly facing each other and in Case 2 the groups are not directly facing each other. Figure 9(a) and (b) shows the trajectory for Case 1 and Case 2, respectively, and Figure 10 shows the snapshots of the whole procedure for Case 1 and Figure 11 gives the snapshots for Case 2.

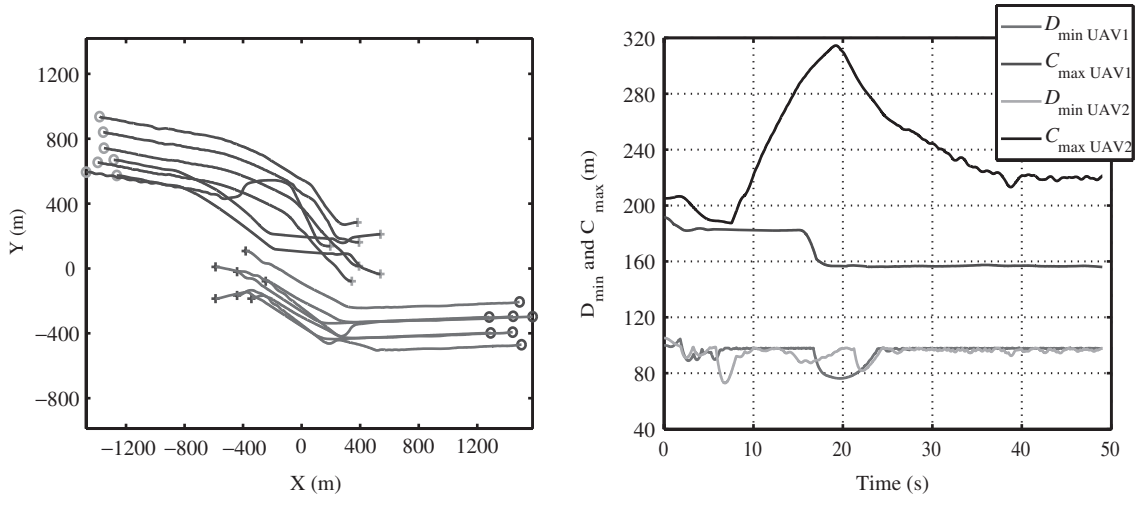

Figure 5. (a) GCA trajectory (b) $D_{\min}$ and $C_{\max}$ for initial $\psi_1 = 0^\circ$ and $\psi_2 = 180^\circ$.

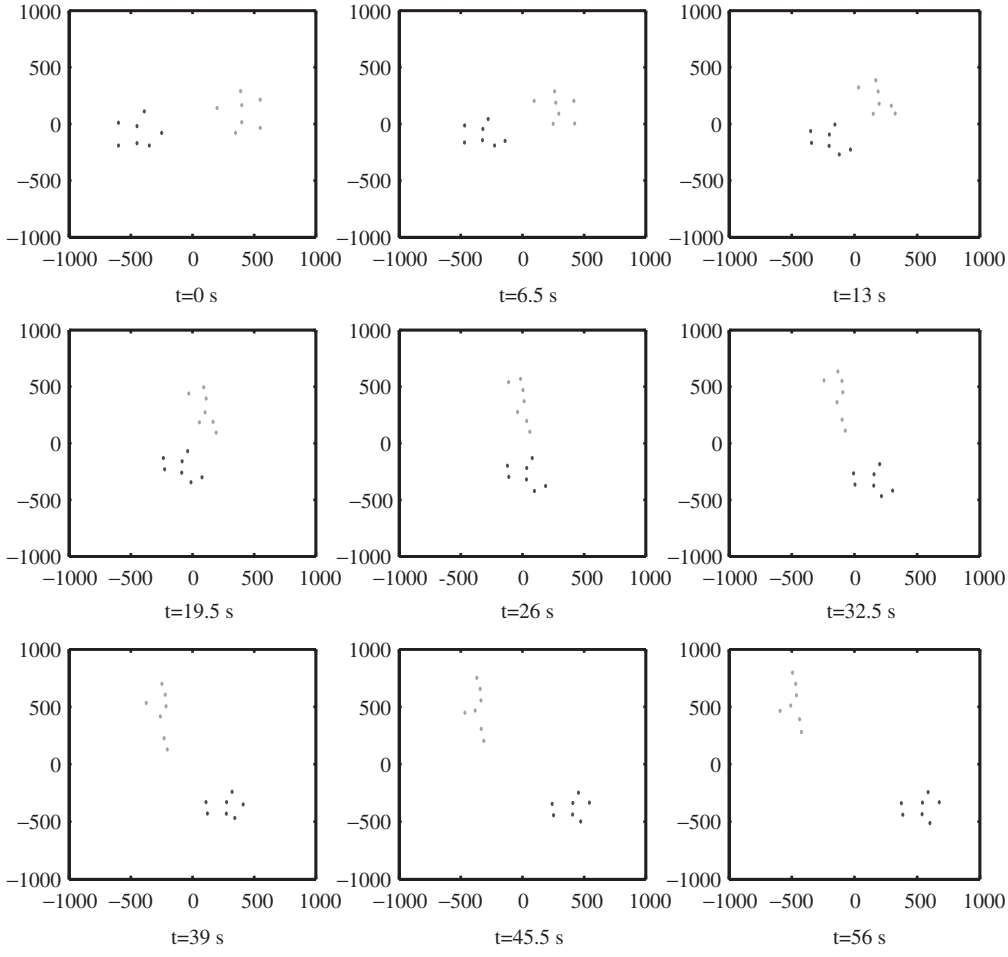

Figure 6. GCA snapshots for initial $\psi_1 = 0^\circ$ and $\psi_2 = 180^\circ$.

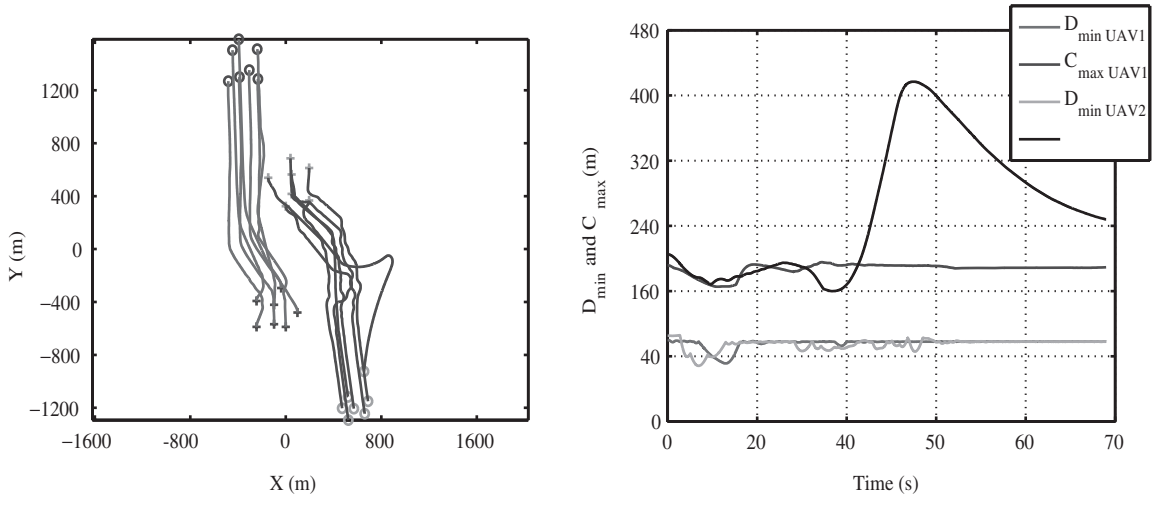

Figure 7. (a) GCA trajectory (b) $D_{\min}$ and $C_{\max}$ for initial $\psi_1 = 90^\circ$ and $\psi_2 = 270^\circ$.

These experimental results in 2D plane show that, with the help of different basic swarming laws, different complex group behaviours like group-wise and ICA can be achieved. In group-wise collision avoidance, there is a large deviation in heading from its normal heading in comparison to ICA. In ICA the sensor range required to achieve avoidance is high, whereas group collision can be achieved at low sensor ranges.

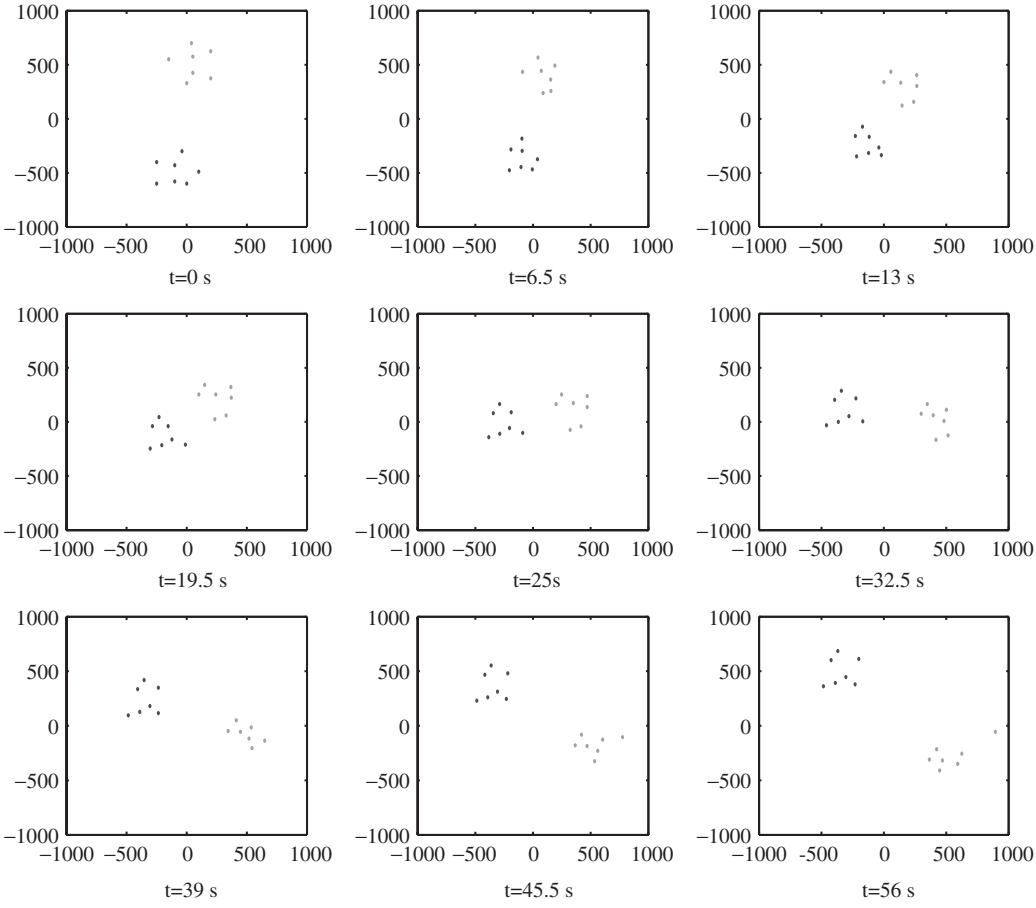

Figure 8. GCA snapshots for initial $\psi_1 = 90^\circ$ and $\psi_2 = 270^\circ$.

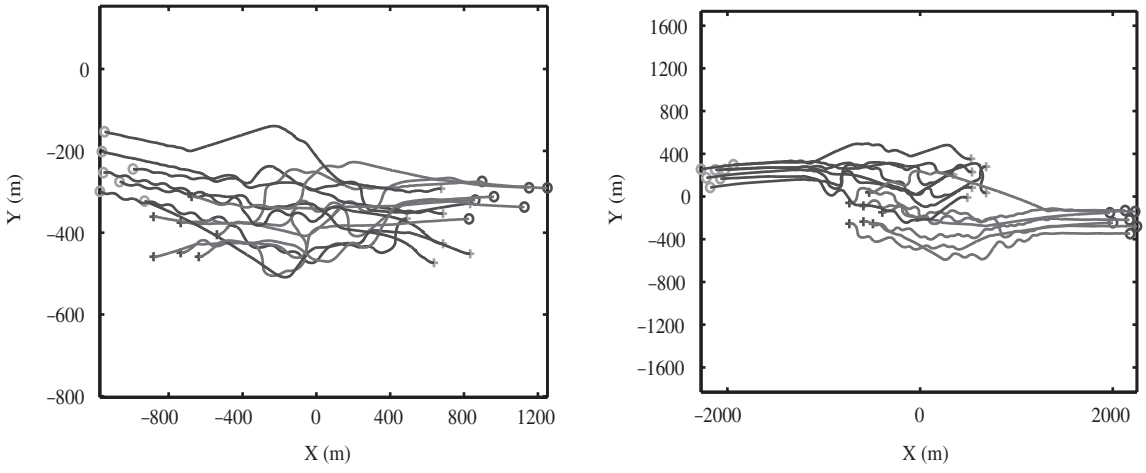

Figure 9. (a) ICA trajectory Case 1 (b) ICA trajectory for Case 2.

5.2. *3D collision avoidance*

In this section, we experimentally illustrate the anayltical result obtained earlier, to the effect that when the cohesion rule is applied, all the UAVs settle down at a constant altitude on a circle of constant radius. Subsequently, several simulation experiments are conducted to validate the algorithms developed for two kinds of collision avoidance problems in the

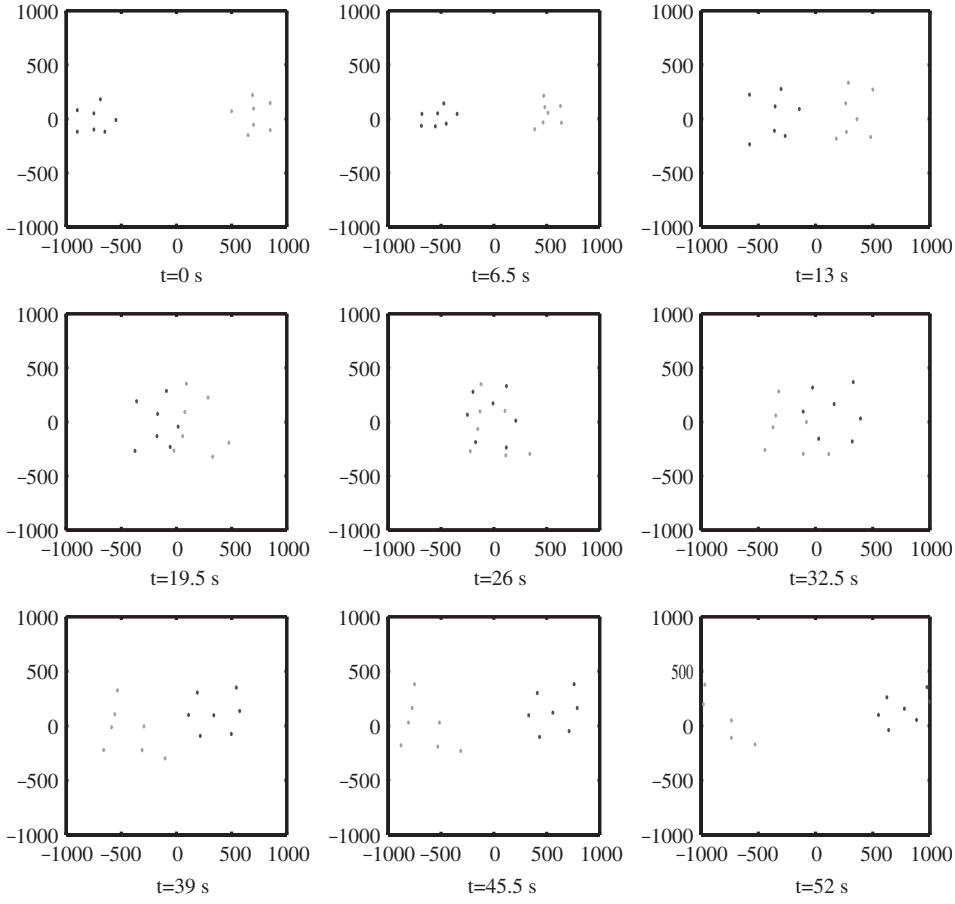

Figure 10. ICA snapshots for Case 1.

3D plane. The effect of various parameters on three group collision schemes developed earlier, and on ICA, is also shown with the help of simulations.

When the cohesion rule is applied, all the UAVs settle at the same altitude in a circular trajectory of constant radius (Figure 12a). For all the UAVs, the pitch angles (Figure 12b) and the vertical accelerations (Figure 13a) become zero and the absolute value of the horizontal acceleration becomes constant (Figure 13b).

Simulations are also carried out to study the effect of w_c, w_d and w_h on the flock size. In the first case, the homing rule weight is kept constant ($w_h = 0.5$), and for a particular value of w_d, w_c is varied from 0.1 to 1. Figure 14(a) shows that the flock size first decreases with w_c and then increases. The reason behind decrease in size is that the 'cohesion rule' is attractive in nature but the subsequent increase in size with w_c happens because of the loss of stability. In the second case (Figure 14b), at $w_d = 0.5$ and for different values of w_h and w_c, variation of flock size is plotted. The same trend as in Figure 14(a) can be observed, but it can also be seen that the flock size increases with the value of w_h because the cohesion effect is being reduced with increase in w_h. It was found that the value of w_c, between 0.2 and 0.4, is appropriate for small flock size and stability.

Let the coordinates of the first group be (X_1, Y_1, Z_1) and the coordinates of the second group be $(X_1 - X_D, Y_1 - Y_D, Z_1 - Z_D)$, where X_D, Y_D and Z_D are constants. With the help of these constants, position of the second group can be varied along the three axes. Several simulations were carried out to check the effectiveness of the three group-wise collision avoidance schemes discussed earlier by varying these constants. Scheme 1 is the basic scheme, Scheme 2 is the cohesion enhancement scheme and Scheme 3 is the conflict free scheme. The important simulation parameters assumed are $\rho_{fix} = 600\,\text{m}$, $d_{min} = 100\,\text{m}$, $V = 20\,\text{m}^{-1}\,\text{s}$, $H_{min} = 600\,\text{m}$, $V_{min} = 300\,\text{m}$, $X_D = 600\,\text{m}$, and $Y_D = 0\,\text{m}$. The rule weights when no alien UAV is the detected are $w_c = 0.4$, $w_h = 0.7$, $w_d = 0.5$, $w_f = 0.1$, $w_{av} = 0$ and the rule weights when alien UAVs are detected are $w_c = 0.2$, $w_h = 0.35$, $w_d = 0.5$, $w_f = 0.2$, $w_{av} = 0.5$. The abbreviations used in Table 1 are C = Collision, CA = Collision Avoidance and GCA = Group-wise Collision Avoidance.

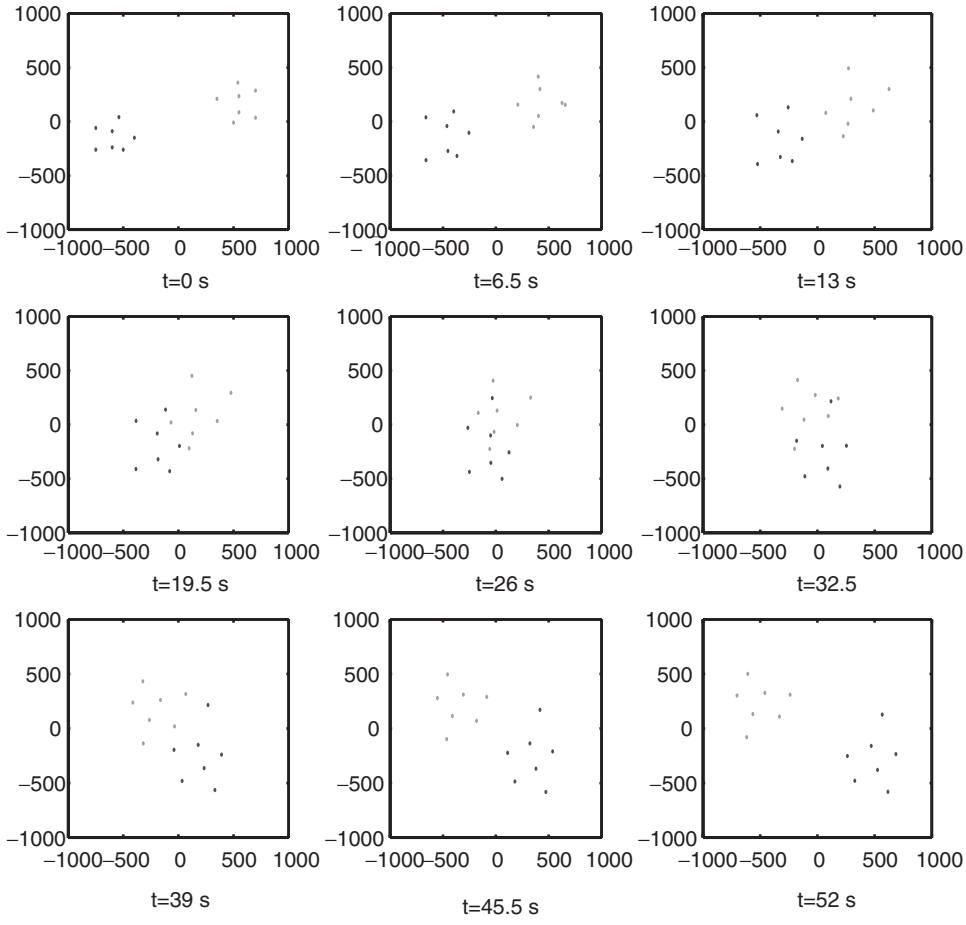

Figure 11. ICA snapshots for Case 2.

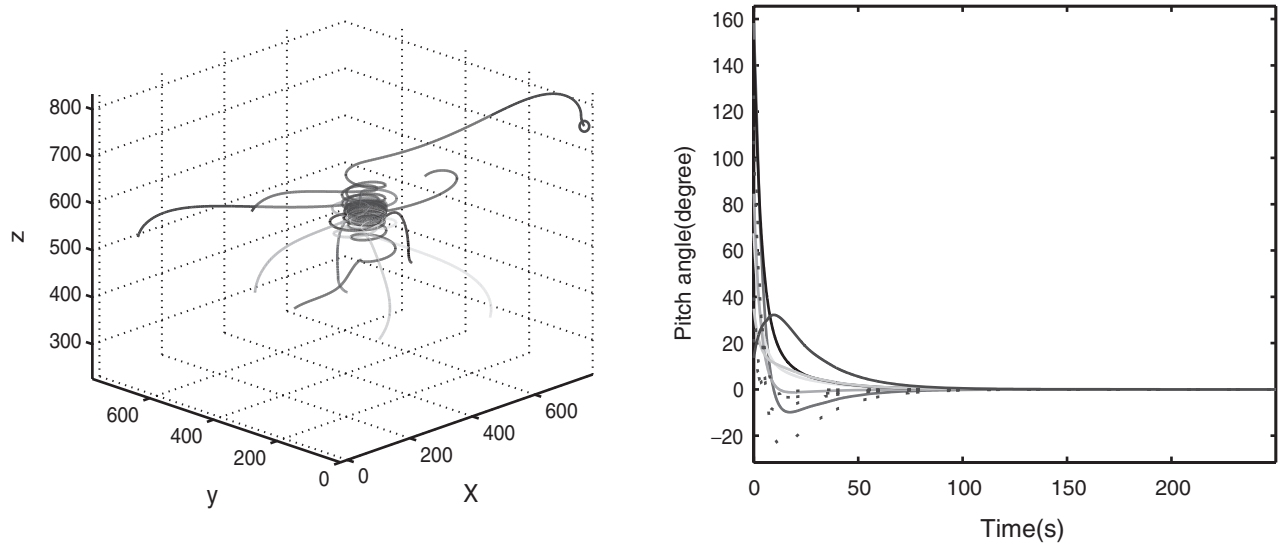

Figure 12. (a) Trajectory (only cohesion) and (b) Variation of pitch angle.

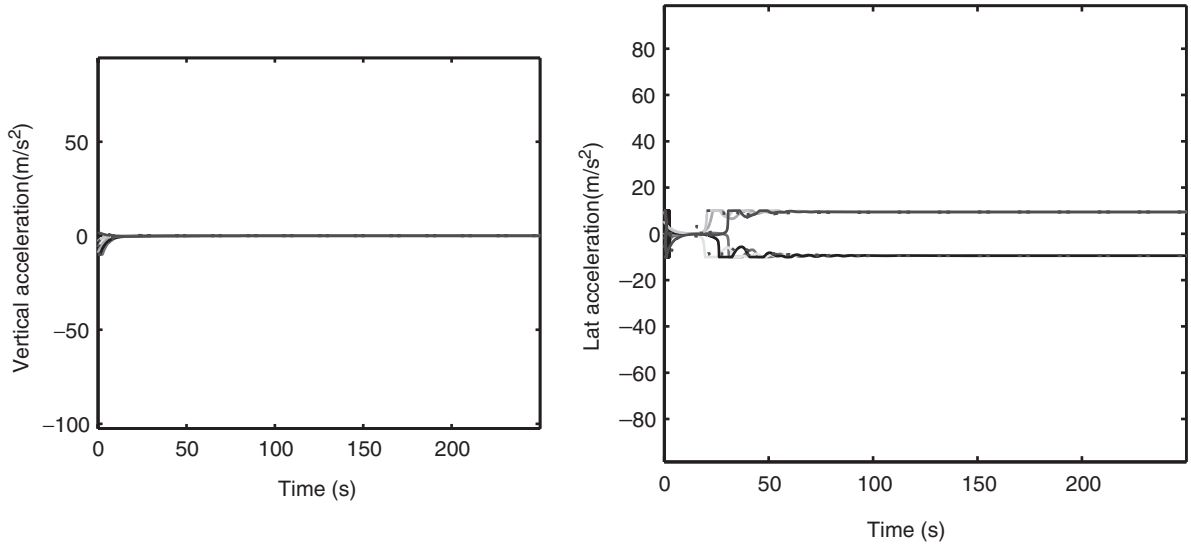

Figure 13. (a) Vertical and (b) horizontal component of acceleration.

Figure 15(a) and (b) shows trajectories for GCA for $Z_D = 50$ and $Z_D = 25$, respectively. For $Z_D = 25$, in Scheme 1, collision is avoided but the group structure is not maintained (Figure 15b). One of the UAVs leaves the group while performing collision avoidance and then again rejoins the group. Now, with the same $Z_D = 25$, Scheme 2 is applied and the collision avoidance is seen to be group-wise (Figure 16a). Table 1 shows that below $Z_D = 25$, Scheme 2 fails (see Figure 16b). The reason for failure is that the time available for the group-wise collision avoidance is less because avoidance angle calculated by the algorithm is opposite in sign when compared to the other group members for performing collision avoidance. Simulation results (Figures 17 and 18) show that Scheme 3 is versatile and robust enough in achieving the GCA for various initial conditions and different detection sensor ranges. Figure 19(a) and (b) shows the effect of sensor range on average heading and average pitch angle, respectively.

ICA trajectories for $\rho = 600\,\text{m}$, $Z_\text{d} = 15\,\text{m}$ and $\rho = 600\,\text{m}$, $Z_\text{d} = 0\,\text{m}$, is shown in Figure 20(a) and (b), respectively. To check the effect of sensor range, reduced values of ρ are used and results are plotted here. Figure 21(a) shows the trajectory for $\rho = 400\,\text{m}$ and Figure 21(b) shows the trajectory for $\rho = 300\,\text{m}$. Figure 22(a) and (b) shows the average heading and pitch when sensor range is reduced from 600 to 300 m.

Experimental results included in this section clearly support the analysis done earlier of the phenomena of settling down of all the UAVs at constant altitude on a circle of constant radius, when the cohesion rule is applied. It is observed that for $w_\text{d} = 0.5$, w_c between 0.2 and 0.4 is appropriate for small flock size and stability. Results also show that the conflict free scheme achieves GCA for all initial conditions. It is observed that ICA does not give satisfactory results for $\rho < 400\,\text{m}$, whereas group collision avoidance performed well even for $\rho = 150\,\text{m}$.

5.3. *Effect of position uncertainty*

In this section, we study the effect of position uncertainty on group behaviour and both kind of collision avoidance schemes. The two parameters D_min and C_max are used to study the effects of position uncertainty. As defined earlier, D_min is the minimum distance between two UAVs in a group, and a nonzero D_min ensures that there is no collision between the two UAVs. C_max, on other hand, is the maximum distance of any UAV in the group from the centroid. If this quantity is less then the sensor range is ρ and the group is said to be stable. Positional uncertainty is modelled as a zero mean normally distributed process with standard deviation (σ) up to 40 m. This noise is added to the position of all the UAVs in the simulations. The plots shown are only for group-wise collision avoidance. Figure 23(a) shows that D_min is above 20 m up to $\sigma = 30\,\text{m}$. Figure 23(b) shows that C_max is well below the value of the sensor range ($\rho = 600\,\text{m}$) for all the values of σ. Table 2 summarises the result for both schemes and shows that GCA is successful in terms of D_min and C_max for up to $\sigma = 30\,\text{m}$ and ICA up to $\sigma = 20\,\text{m}$.

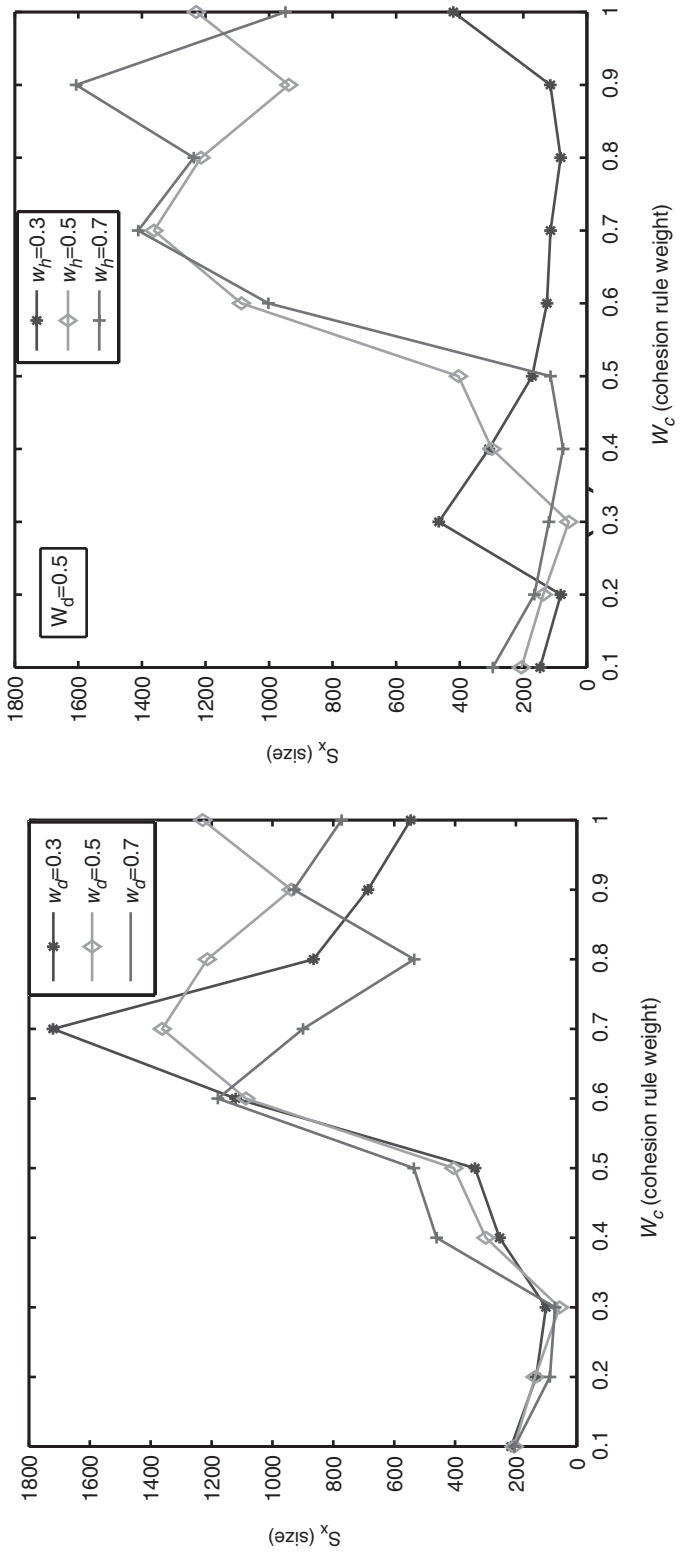

Figure 14. (a) Effect of w_c and w_d on cluster size. (b) Effect of w_c and w_h on cluster size.

Table 1. GCA for different Z_D.

Sr No	Z_D	Scheme 1	Scheme 2	Scheme 3
1	0	C	C	G C A
2	5	C	C	G C A
2	10	C	C	G C A
4	15	C	C	G C A
5	20	C	C	G C A
6	25	C A	G C A	G C A
7	30	C A	G C A	G C A
8	35	C A	G C A	G C A
9	40	C A	G C A	G C A
10	45	C A	G C A	G C A
11	50	G C A	G C A	G C A

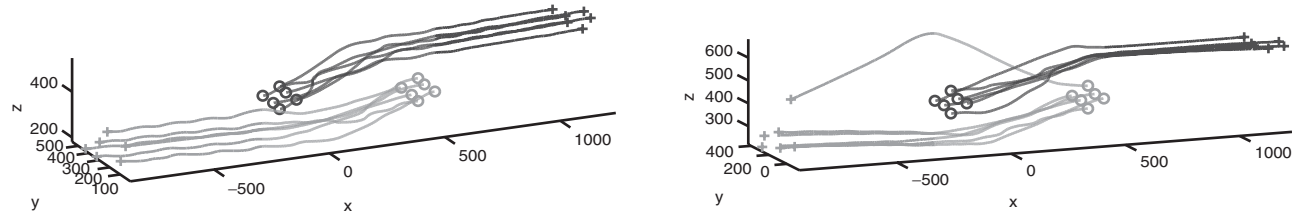

Figure 15. (a) $Z_D = 50$ (Scheme 1) and (b) $Z_D = 25$ (Scheme 1).

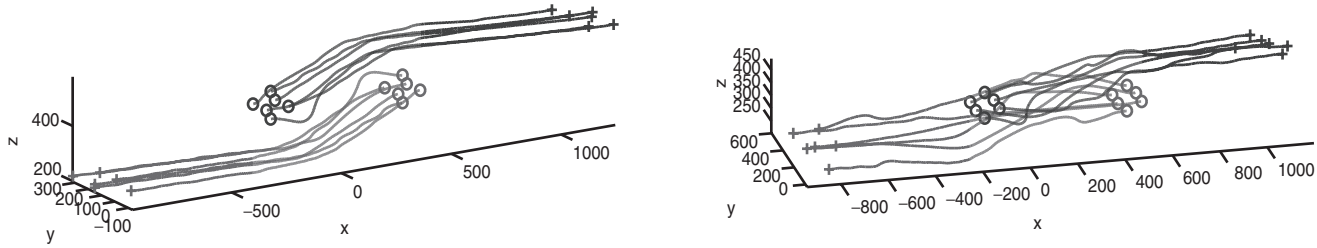

Figure 16. (a) $Z_D = 25$ (Scheme 2) and (b) $Z_D = 20$ (Scheme 2).

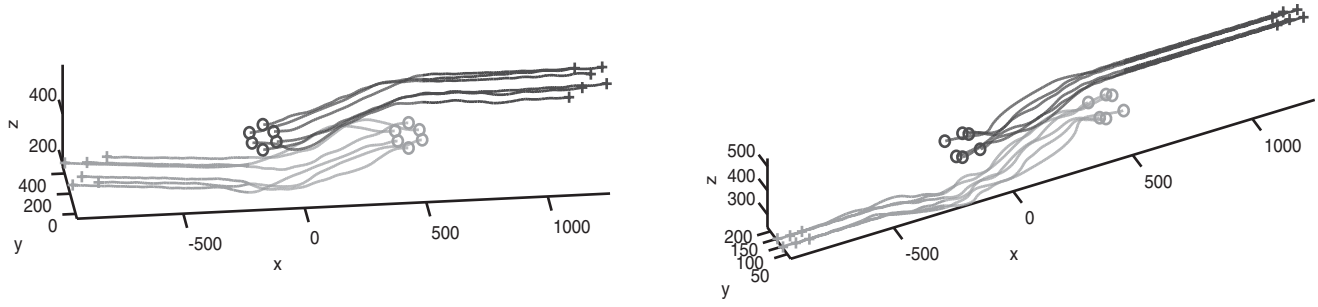

Figure 17. Scheme 3: $Z_D = 20$ (a) $\rho = 600$, $d_{min} = 100$ and (b) $\rho = 300$, $d_{min} = 50$.

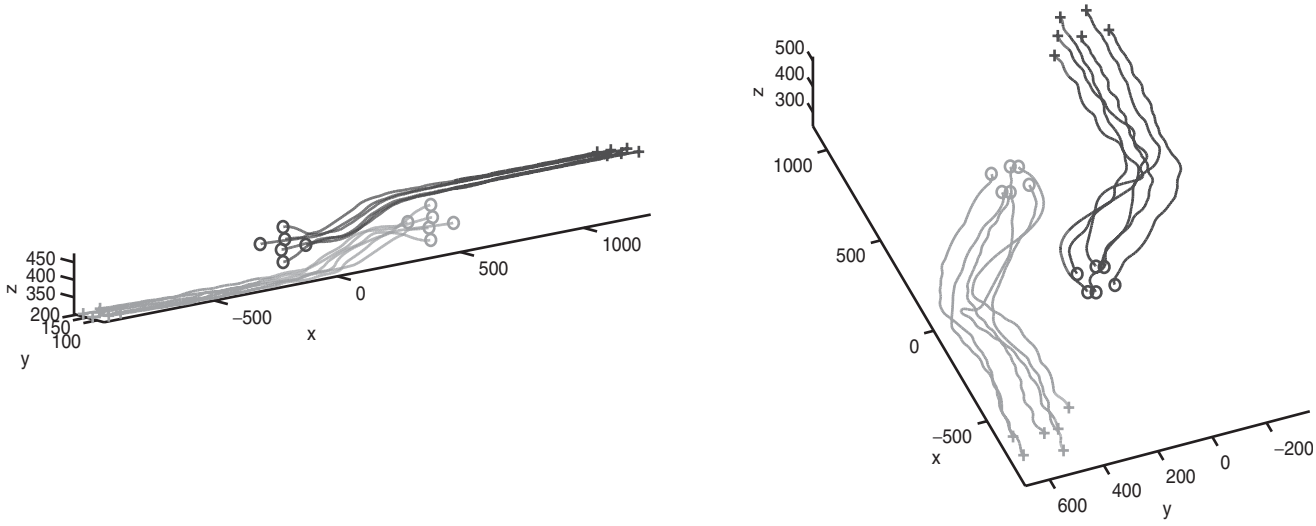

Figure 18. Scheme 3 (a) $Z_D = 20$, $\rho = 150$, $d_{min} = 50$ and (b) $Z_D = 10$, $\rho = 600$, $d_{min} = 100$, $Y_D = -80$.

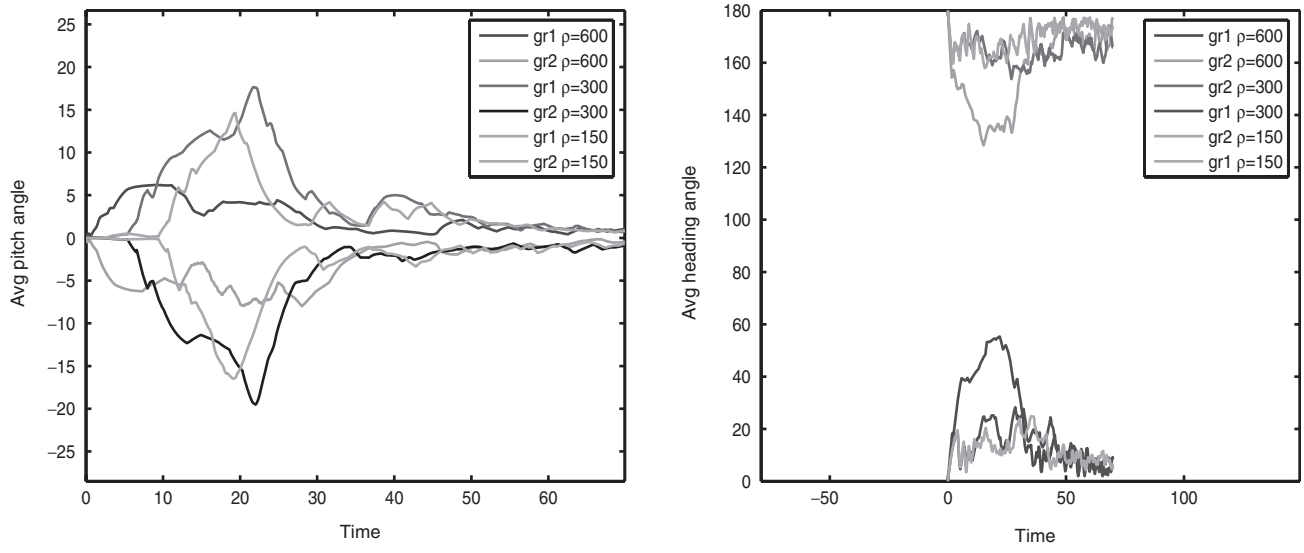

Figure 19. (a) Average pitch angle and (b) Average heading angle.

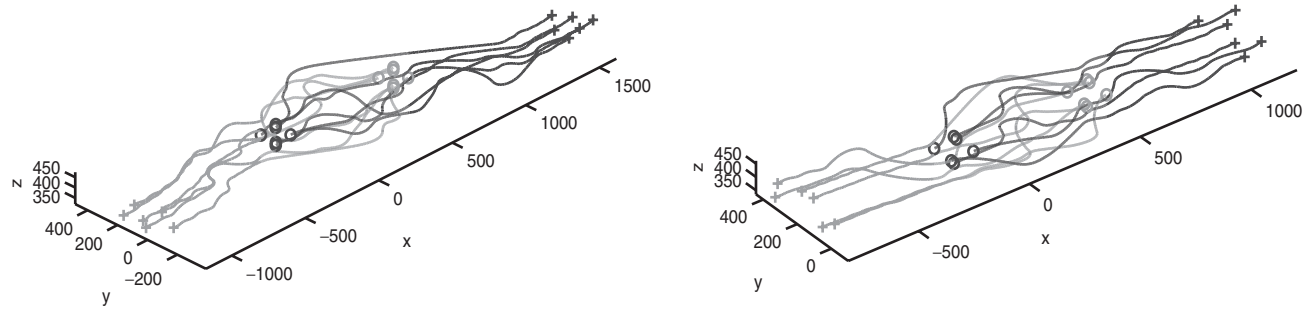

Figure 20. ICA: (a) $Z_D = 15$ and (b) $Z_D = 0$.

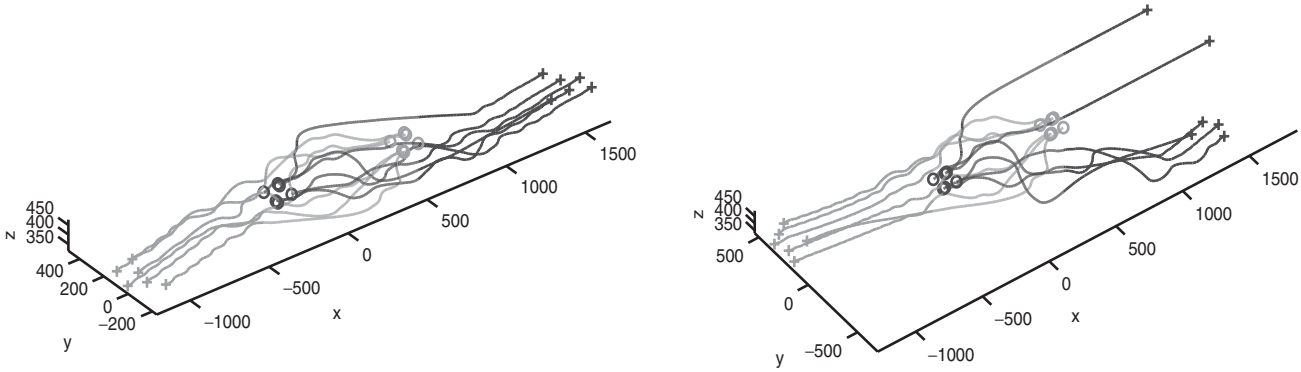

Figure 21. ICA: (a) $\rho = 400\,\text{m}$ and (b) $\rho = 300\,\text{m}$.

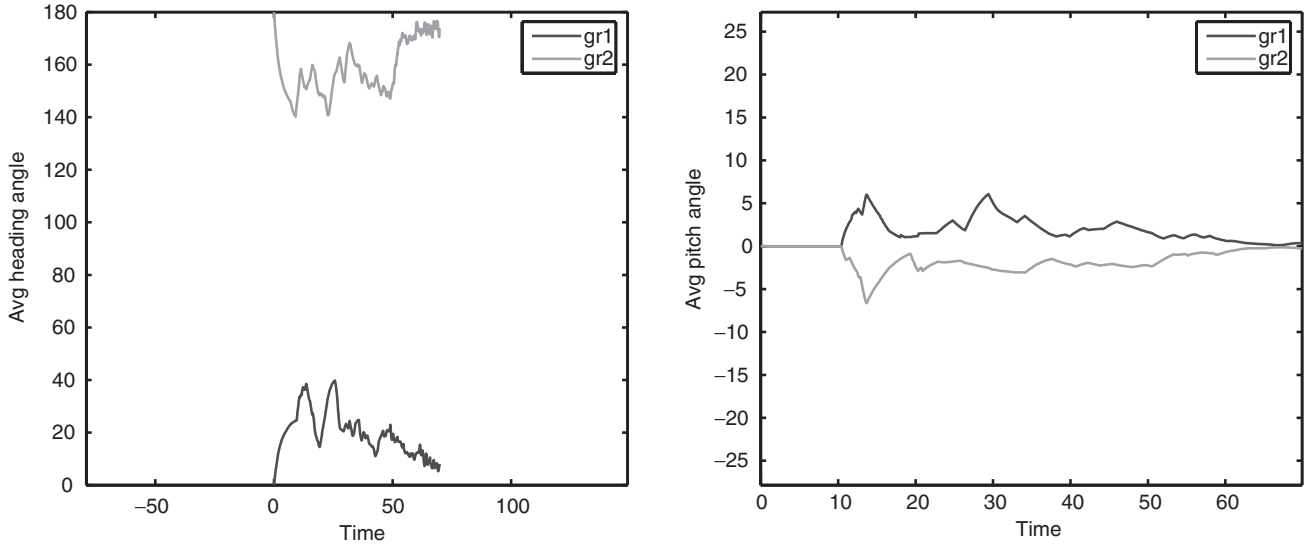

Figure 22. ICA: (a) Average heading angle and (b) Average pitch angle.

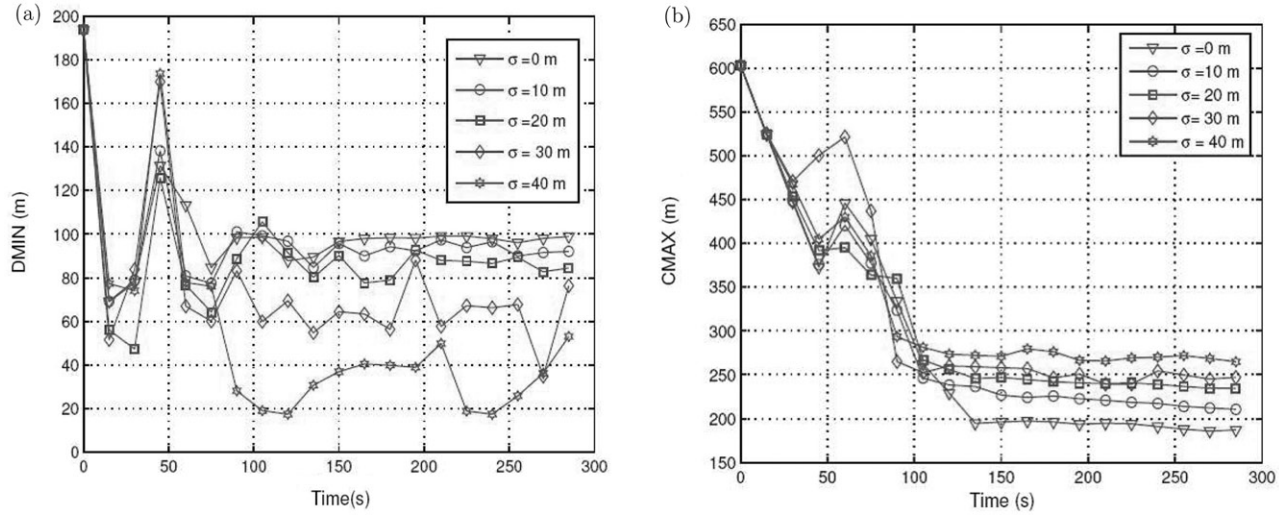

Figure 23. (a) Effect of position uncertainty on $D_{\min}$ in GCA and (b) Effect of position uncertainty on $C_{\max}$ in GCA.

Table 2. Effect of position uncertainty on GCA and ICA.

Scheme	$\sigma = 0$	$\sigma = 10$	$\sigma = 20$	$\sigma = 30$	$\sigma = 40$
GCA	Yes	Yes	Yes	Yes	No
ICA	Yes	Yes	Yes	No	No

6. Conclusions

In this article, various basic swarming algorithms for UAVs have been successfully developed both in the 2D and the 3D cases. The effect of these basic laws has been studied on the group behaviour of UAV swarms. Algorithms are developed and successfully tested for the two types of collision avoidance, group-wise and individual, both in the 2-D and the 3-D. Three different schemes are subsequently formulated for GCA in the 3D plane. Simulation results show that in a conflict free scheme, group collision is achieved successfully for all the initial conditions. Simulation results show that, in GCA, the total deviation from the required path is very high in comparison to the ICA scheme. It can also be observed that the sensor range required to achieve the ICA is high, whereas the group collision can be achieved at low sensor ranges also. It is shown both analytically and with the help of simulations that, when the cohesion rule is applied, an equilibrium condition is reached in which all the UAVs settle at a constant altitude on a circle of constant radius. It is also proved analytically that this equilibrium condition is stable for all values of velocity V and acceleration constant k. The effect of w_c, w_d and w_h on the size and stability of the swarm has been studied. Simulation results show that for both w_d and w_h are between 0.5 and 0.7 and w_c is between 0.2 and 0.3, size and stability of the group is maintained.

References

Beard, R.W. (2007), 'State Estimation for Micro Air Vehicles', *Studies in Computational Intelligence*, 70, 173–199.

Bonabeau, E., and Theraulaz, G. (1997), 'Self-organisation in Social Insects', *Trends in Ecology and Evolution*, 12, 188–193.

Chang, S.P., and Min, J.T. (2003), 'Multiple Aerial Vehicle Formation using Swarm Intelligence', in *AIAA Guidance, Navigation, and Control Conference and Exhibit*, Austin, Texas.

Chang, D., Shadden, S., Marsden, J., and Olfati-Saber, R. (2003), 'Collision Avoidance for Multiple Agent Systems', in *Proceedings of the 42nd IEEE Conference on Decision and Control*, Maui, Hawaii.

Crowther, B. (2004), 'Rule-based Guidance for Flight Vehicle Flocking', *Proceedings of the Institute of Mechanical Engineers, Part G: Journal of Aerospace Engineering*, 218(2), 111–124.

Glen, A.D., and Michael, S.S. (2003), 'The Aerodynamic Benefits of Self-organising in Bird Flocks', in *41st Aerospace Sciences Meeting and Exhibit*, Reno, Neveda. January 2003.

Jain, L.C., Quteishat, A., and Lim, C.P. (2007), 'Intelligent Machines: an Introducion', *Studies in Computational Intelligence*, 70, 1–9.

Jha, P.K., and Ghose, D. (2003), 'Avoidance Between Cluster of UAVs', *Proc of Intl. Conference on Computational Intelligence, Robotics and Autonomous Systems*, Singapore.

Reynolds, C. (1987), 'Flocks, Herds and Schools: A Distributed Behavioural Model', *Computer Graphics*, 21(4), 25–34.

Shanmugavel, M., Tsourdos, A., White, B.A., and Zbikowski, R. (2007), 'Differential Geometric Path Planning of Multiple UAVs', *AsME Journal of Dynamic Systems, Measurements, and Control*, 129(5), 620–632.

Sujit, P.B., and Beard, R.W. (2007), 'Multiple MAV Task Allocation using Distributed Auctions', in *Proceedings of AIAA Guidance, Navigation, and Control Conference and Exhibit*, Hilton Head, South Carolina.

Tanner, G., Jadbabaie, A., and Pappas, J. (2003), 'Stable Flocking of Mobile Agents, Part I: Fixed Topology, Part II: Dynamic Topology', in *42nd IEEE Conference on Decision and Control*, Maui, Hawaii, pp. 2010–2021.

Yasuaki, A., and Yoshiki, M. (2001), 'Collision Avoidance Method for Multiple Autonomous Mobile Agents by Implicit Cooperation', in *Proceedings of the IEEE/RSJ International Conference on Intelligent Robots and Systems*, Maui, Hawaii, USA.